Soft Matter

PAPER

View Article Online
View Journal | View Issue

Cite this: *Soft Matter*, 2020, **16**, 4502

Proving and interpreting the spontaneous formation of bulk nanobubbles in aqueous organic solvent solutions: effects of solvent type and content†

Ananda J. Jadhav and Mostafa Barigou *

We show that the mixing of organic solvents with pure water leads to the spontaneous formation of suspended nano-entities which exhibit long-term stability on the scale of months. A wide range of solvents representing different functional groups are studied: methanol, ethanol, propanol, acetone, DMSO and formamide. We use various physical and chemical analytical techniques to provide compounded evidence that the nano-entities observed in all these aqueous solvent solutions must be gas-filled nanobubbles as they cannot be attributed to solvent nanodroplets, impurities or contamination. The nanobubble suspensions are characterized in terms of their bubble size distribution, bubble number density and zeta potential. The bubble number density achieved is a function of the type of solvent. It increases sharply with solvent content, reaching a maximum at an intermediate solvent concentration, before falling off to zero. We show that, whilst bulk nanobubbles can exist in pure water, they cannot exist in pure organic solvents and they disappear at some organic solvent-water ratio depending on the type of solvent. The gas solubility of the solvent relative to water as well as the molecular structure of the solvent are determining factors in the formation and stability of bulk nanobubbles. These phenomena are discussed and interpreted in the light of the experimental results obtained.

Received 17th January 2020,
Accepted 15th April 2020

DOI: 10.1039/d0sm00111b

rsc.li/soft-matter-journal

1. Introduction

Bulk nanobubbles (BNBs) are an emerging field which is attracting much attention from researchers and industrial practitioners alike. Their existence has been reported in a number of recent experimental studies[1–4] and strong indirect evidence has been provided to show that such nano-entities must be gas bubbles.[5,6] Nonetheless, considerable speculation and controversy still exist about the existence and nature of BNBs, their origin and their extraordinary longevity which contradicts predictions of the diffusive gas transport based on the Epstein and Plesset theory.[7] Those who dispute the existence of BNBs tend to attribute them to supra-molecular structures, solvent or oil nanodroplets or simply impurities and contamination, based on either questionable experimentation or sheer speculation.[8–15] A similar debate which lasted for many years took place after surface nanobubbles emerged and became the focus of attention about two decades ago.[16] The present situation is exacerbated by the lack of a full rational explanation of the mechanism behind the long-term stability of BNBs.[6,17–19] A number of speculative interpretations have been postulated but a complete physical model has yet to emerge.

Despite such scepticism, however, many applications have been suggested for BNBs, including control of the nucleation mechanism in cavitation/boiling,[20] facilitating oxygen supply to marine/aquatic life (plant and fish),[21] detoxification of water,[3,22] enhanced remediation of organic contaminants,[23] drag reduction,[24] prevention of surface fouling,[25,26] enhanced ultrasound imaging of small cell lung cancer,[27–29] oxygenation of hypoxic conditions for cardiac resuscitation,[30] enhanced seed germination,[31,32] and improved efficiency of IC engines.[33,34] This nonexhaustive list highlights the wide and versatile interest in BNBs. BNBs offer significant advantages over microbubbles due to their persistence, negligible buoyancy and huge relative surface area. However, it is still not understood how they can be produced in an efficient, consistent and controlled fashion, especially in large volumes, and how they can be efficiently exploited in all the pertinent technologies.

Various techniques have been suggested for BNB production, including hydrodynamic and acoustic cavitation,[6,18,35–38] fluidic oscillation,[39] and nano-membrane filtration.[40] These methods suffer from a number of drawbacks as they tend to be energy intensive; they are prone to contamination arising from detachment

School of Chemical Engineering, University of Birmingham, Edgbaston, Birmingham, B15 2TT, UK. E-mail: m.barigou@bham.ac.uk

† Electronic supplementary information (ESI) available. See DOI: 10.1039/d0sm00111b

of nanoparticles from surfaces; they lack control of bubble size, uniformity and concentration; and have low resistance to corrosive chemicals, which restricts the use of reactive gases and solutions. The method of solvent exchange by which a local supersaturated environment is created, has been widely used in studies of surface nanobubbles,[41–44] but has not been fully exploited in the formation and study of BNBs.

In this paper, we study the spontaneous formation of BNBs resulting from the mixing of pure water with an organic solvent. An extensive range representing different functional groups of aqueous organic solvents is investigated. We use a range of physical and chemical analytical techniques to show that the nano-entities formed must be gas-filled nanobubbles, as follows:

1. In the case of an organic solvent with a lower boiling point than water, we separate the solvent from the nanobubble suspension and analyse the nanobubble size distribution and bubble number density to confirm that they remain unaffected;

2. We use Fourier transform infrared spectroscopy (FT-IR) to analyse and compare the functional groups present in pure water and in nanobubble suspensions;

3. We analyse pure water and nanobubble suspensions using gas chromatography-mass spectroscopy (GC-MS) to examine for any organic contamination;

4. We analyse pure water and nanobubble suspensions using inductive coupled plasma mass spectroscopy (ICP-MS) to detect any inorganic contamination;

5. For each organic solvent considered, we completely evaporate the water and solvent from the nanobubble suspension and examine if there is any residue.

The BNB suspensions are visualized and the nanobubbles measured by a nanoparticle tracking analysis technique, and their surface charge is measured in terms of their zeta potential. We study the influence of the type of solvent and its mole fraction on the existence of BNBs and their bubble number density. We also monitor the long-term stability of the BNB suspensions over a period of over three months. In the light of the experimental results obtained, we address a number of fundamental questions relating to the existence and behaviour of BNBs in aqueous solvent solutions.

2. Experimental section

2.1 Materials

Ultrapure water (type-1), henceforth referred to as simply pure water, from a Millipore purification system (Avidity Science, UK), of electrical conductivity 0.055 μS cm^{-1} and pH 6.7 at a temperature of 20 °C, was used in all experiments. All solvents and reagents used were of the highest purity grade available on the market. All glassware was cleaned by immersion for 30 min in a 10% aqueous solution of potassium hydroxide (KOH, Sigma Aldrich, UK) placed inside an ultrasonic bath, followed by rinsing with ultrapure water, drying in a microwave oven and flushing with a stream of high-purity dry nitrogen gas. Analytical grade (99.9% pure) methanol, ethanol, 2-propanol, acetone, dimethyl sulfoxide (DMSO) and formamide were purchased from Fisher Scientific (UK) and were handled in glassware in order to avoid contamination from plastic products. Prior to experimentation, purified water and all stock solutions were initially examined for any nanoscale entities using the Nanosight instrument (described further below) employed for the measurement of BNBs, and no significant levels of impurity were observed.

2.2 Methods

2.2.1 Formation of BNBs by water–solvent mixing. BNBs were formed by mixing an organic solvent at different concentrations within the range 0.01–0.9 mole fraction with pure water at room temperature, in 100 mL glass beakers, as illustrated in Fig. 1. The order of mixing (*i.e.* adding solvent to water or adding water to solvent) had no effect on the bubble number density or nanobubble size distribution, within experimental error. We selected a range of solvents: methanol, ethanol, propanol, acetone, DMSO and formamide; their physical properties are summarized in Table 1. The BNB suspensions thus formed were stored at room temperature in 20 mL air-tight glass vials for further analysis.

2.2.2 Nanoparticle tracking analysis (NTA). The concentration, mean size, and size distribution of BNB suspensions was measured using nanoparticle tracking analysis (NTA) afforded by a NanoSight instrument (NS300, Malvern, UK), as described in our previous work.[6] Further details are summarised in the ESI.†

2.2.3 Zeta potential. The electrokinetic or zeta potential is a key indicator of the stability of a colloidal dispersion. The zeta potential of the BNB suspensions was measured by a ZEN5600 ZetaSizer Nano ZSP (Malvern Instruments, UK), as described in our previous work;[18] more details are given in the ESI.†

3. Results and discussion

We shall start by assuming that the entities formed in the aqueous solvent solutions are BNBs and make some general observations about their characteristics and behaviour. We will then present multiple pieces of evidence to show that the observed entities are indeed BNBs and not any of the common nano-scale impurities sometimes associated with BNBs. Subsequently, we shall address a number of fundamental questions

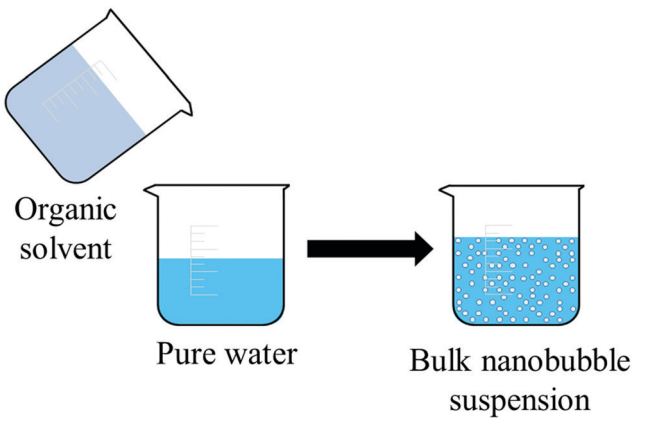

Fig. 1 Schematic representation of BNB generation by mixing of organic solvent and pure water.

Table 1 Physical properties of water and organic solvents

Solvent	Water	Methanol	Ethanol	Propanol	Acetone	DMSO	Formamide
Formula	H_2O			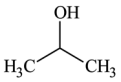			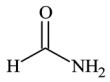
Protic	Yes	Yes	Yes	Yes	No	No	Yes
Dielectric constant (20 °C)	80.2	33.0	25.3	21.8	20.7	47.24	110
Viscosity (mPa s) (25 °C)	0.89	0.543	1.095	1.920	0.316	1.987	3.300
Surface tension (mN m^{-1}) (20 °C)	72.80	22.70	22.10	23.00	25.20	42.92	57.03

relating to the existence of BNBs and their behaviour in aqueous solvent solutions.

3.1 General observations

All the solvents studied exhibited qualitatively similar nanobubble size distributions. Typical nanobubble size distributions in propanol–water mixtures are presented in Fig. 2, showing a flattening of the peak, *i.e.* a reduction in Kurtosis going from leptokurtic to platykurtic distribution as the solvent fraction increases. The bubble number density is an important parameter to compare nanobubble populations formed in different solvent–water mixtures, as shown in Fig. 3. For example, the bubble number density rises sharply to a maximum value of $\sim 2.65 \times 10^9$ bubble mL^{-1} as the propanol mole fraction increases to ~ 0.03 and falls off sharply at higher propanol fractions, reaching zero bubble mL^{-1} at ~ 0.2 mole fraction of propanol. Other organic solvents exhibit a similar trend, with a maximum number of nanobubbles formed at a mole fraction of ~ 0.2 for methanol, ~ 0.06 for ethanol, ~ 0.05 for acetone, ~ 0.1 for DMSO and ~ 0.05 for formamide, falling off to zero thereafter, as depicted in Fig. 3.

The variations of the number mean bubble diameter are also presented in Fig. 3. The mean bubble diameter generally increases with solvent mole fraction up to the point where the maximum bubble number density is reached. Beyond that point, different solvents exhibit different trends which cannot be easily explained without a more detailed study.

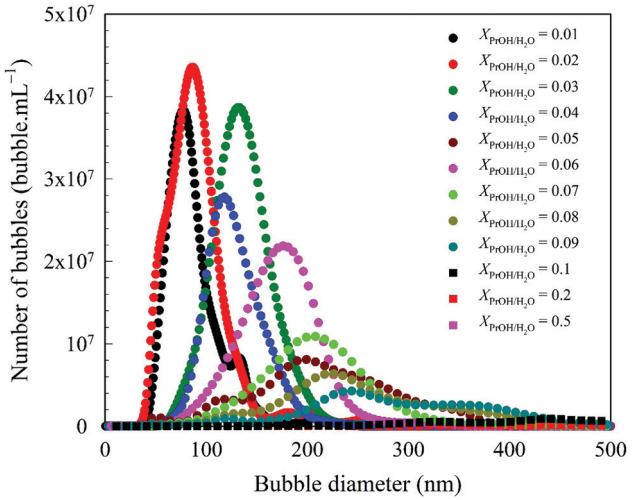

Fig. 2 Typical bulk nanobubble size distributions in propanol–water mixtures.

3.2 Evidence of existence of BNBs in aqueous organic solvent solutions

3.2.1 Solvent separation from BNB suspensions. A rotary vacuum evaporation experiment was conducted to study what happens when the solvent is separated from a BNB suspension, as described in the ESI† and schematically illustrated in Fig. S1 (ESI†). The distillate in the condensing flask and the residue liquid in the evaporation flask were analysed using the NTA technique. Due to the lower boiling points of methanol, ethanol, propanol and acetone than water, these solvents were vaporised, condensed and collected in the receiving flask. Complete separation of the entire solvent did not affect the size distribution or the number density of the BNBs in the remaining solvent-free suspension, as shown in Fig. 4. Due to the higher boiling point of DMSO and formamide, water instead was vaporised, condensed and collected in the receiving flask. In this case, the nanobubbles disappeared completely and were not detected in either the vaporised water or remaining solvent. These experiments answer one of the important questions, namely that the observed nano-entities are not solvent nanodroplets.

3.2.2 Fourier transform infrared spectroscopy (FT-IR) of BNB suspensions. The purity of the BNB suspensions was examined by FT-IR anaylsis. Details of the procedure are given in the ESI.† The FT-IR spectra obtained for pure water and for each pure solvent and its corresponding BNB suspension are presented in Fig. 5. The FT-IR spectrum for pure water exhibits two intense bands at 3300 cm^{-1} caused by O–H stretching, and at 1635 cm^{-1} caused by O–H–O scissors bending. In addition, a smaller band is displayed at 2120 cm^{-1}, a result of the coupling of the scissors-bending and a broad liberation band in the near infrared.[45,46] Any FT-IR detectable foreign substance, *i.e.* any bonded and/or free organic, inorganic and metal impurity is expected to show as an extra peak. Thus, the absence of any extra peaks confirms that the water used contained no detectable contamination.

The water–solvent BNB suspensions exhibit extra peaks, as shown in Fig. 5. The three alcohols display three extra peaks representing in order from left to right, the O–H stretching mode, the C–O stretching mode and the C–C stretching mode, which together indicate in each case the presence of either methanol, ethanol or propanol. Similarly, acetone exhibits three characteristic peaks representing in turn, the C=O stretching mode, the CH_3 bending mode and the C–C–C stretching mode, which together indicate the presence of acetone. DMSO, on the other hand, presents a characteristic peak representing the

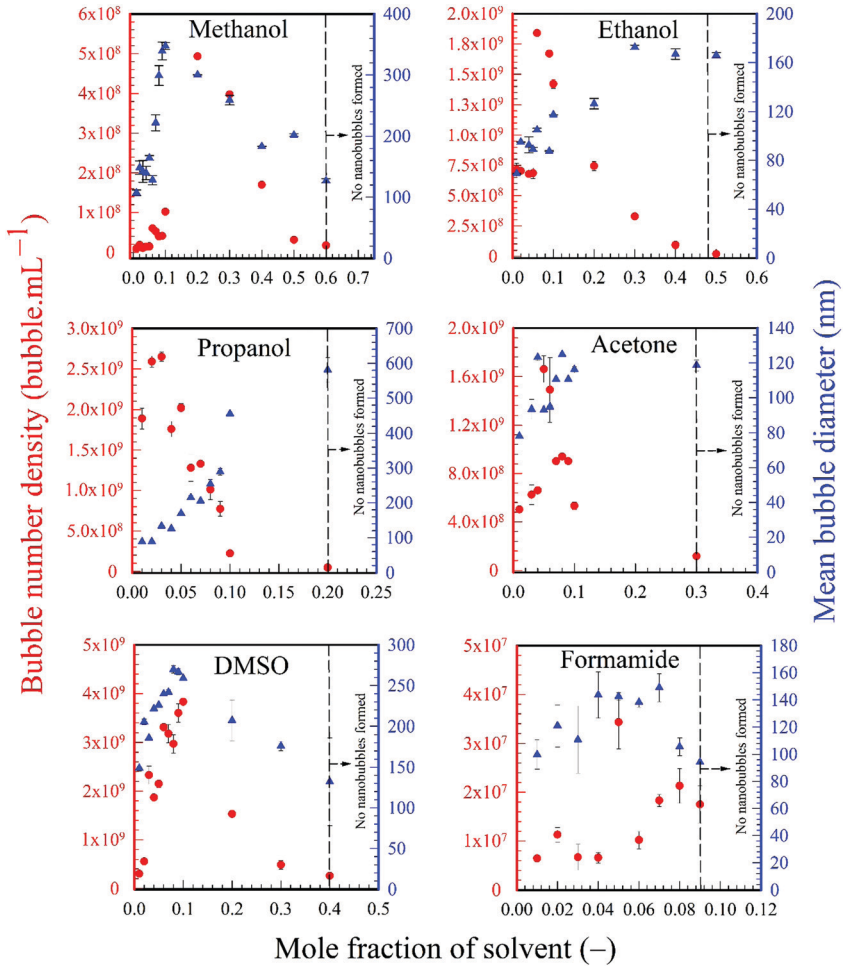

Fig. 3 Variation of bubble number density and mean bubble size as a function of solvent mole fraction.

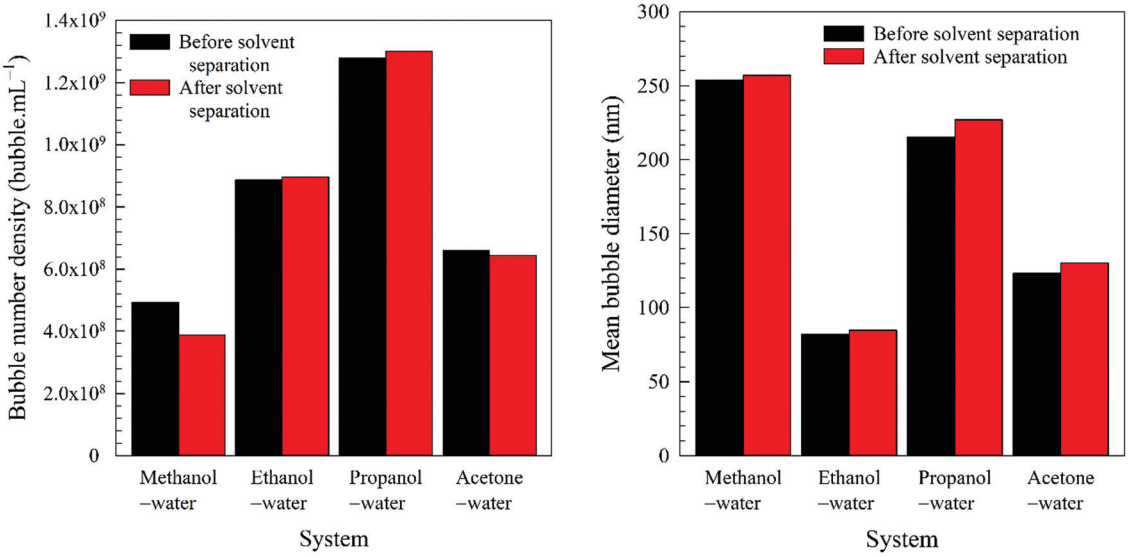

Fig. 4 Bubble number density and mean bubble diameter of BNBs in aqueous solvent solution and after complete separation of solvent from solution.

S=O stretching mode which indicates the presence of DMSO. Finally, formamide presents six characteristic peaks representing, respectively, the symmetric NH_2 stretching mode, the C–H stretching mode, the NH_2 scissoring mode, the C–H bending mode, C–N stretching mode and the C–O stretching mode, which together indicate the presence of formamide.

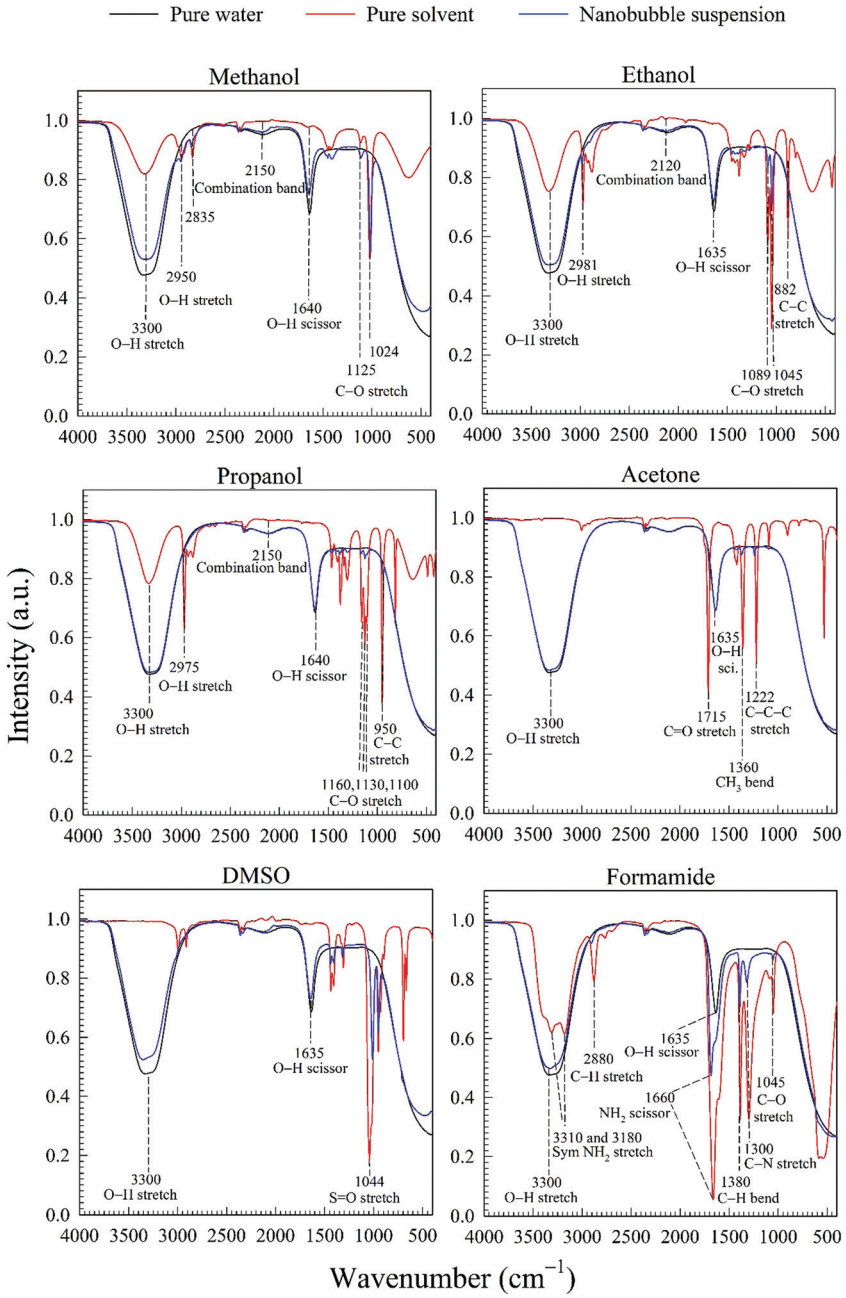

Fig. 5 FTIR results for pure water, pure solvents and corresponding BNB suspensions.

To confirm that these extra peaks do not mask the presence of other chemical compounds of similar functional groups, we conducted the same FT-IR analysis on the collected water after complete separation of the solvents in the rotary evaporator, using the procedure described above. All of the extra peaks disappeared, and the corresponding FT-IR spectrum coincided with that of pure water. In conclusion, therefore, the nano-entities observed in the different water–solvent solutions cannot be attributed to any type of FT-IR detectable contamination.

3.2.3 Gas chromatography-mass spectrometry (GC-MS) analysis of BNB suspensions. Here, we use a GC-MS technique, as described in the ESI,† to check for any organic contamination in our purified water and BNB suspensions, as depicted in Fig. 6. The gas chromatogram of pure water shows a peak at a retention time of 5.9 min (Fig. 6a) which is consistent with that reported by other workers.[47] This peak is observed in the chromatographs of all the water–solvent BNB suspensions. The extra peaks exhibited at retention times of 3.69 min, 3.67 min, 3.06 min, 25.66 min and 34.09 min indicate the presence in the BNB suspensions of, respectively, ethanol, propanol, acetone, DMSO and formamide, as confirmed by the mass spectra presented in Fig. 6b–f. These results confirm that there is no organic contamination present in BNB suspensions.

3.2.4 Inductive coupled plasma-mass spectrometry (ICP-MS) analysis of BNB suspensions. The ICP-MS protocol is described in

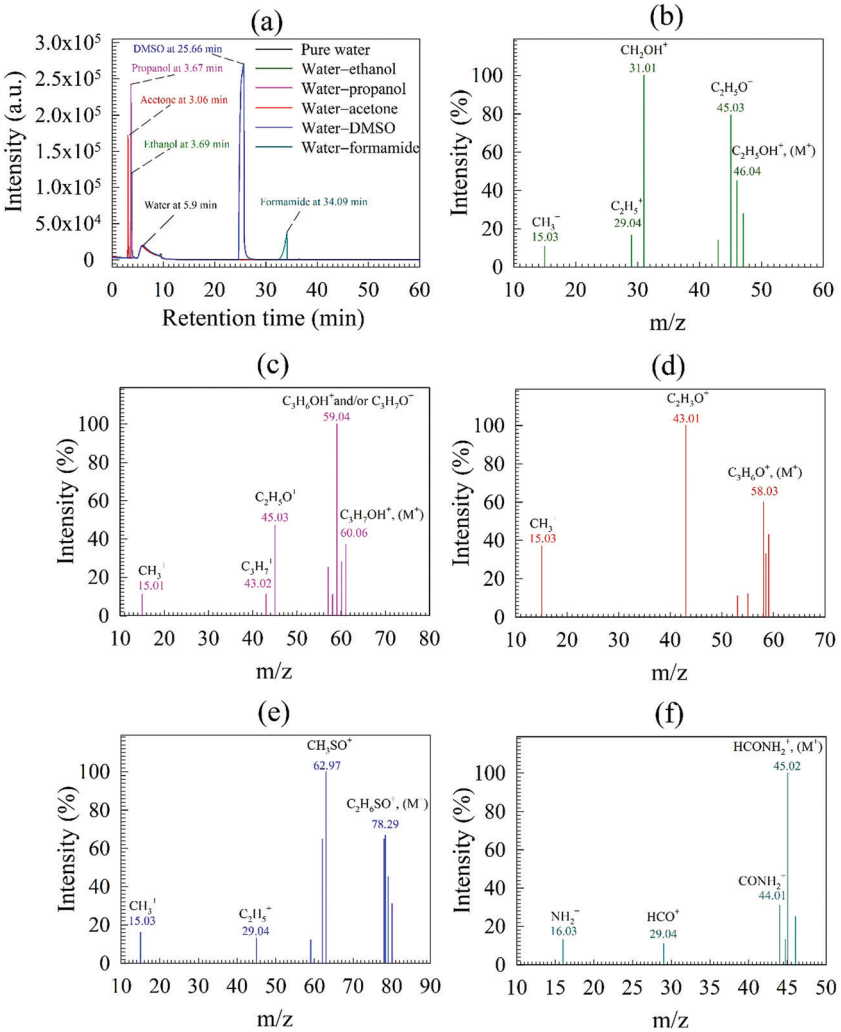

Fig. 6 GC-MS results: (a) chromatogram of pure water and BNB suspensions; mass spectrum of (b) ethanol, (c) propanol, (d) acetone, (e) DMSO, and (f) formamide.

the ESI.† We analysed for 32 metals both in pure water and the BNB suspensions. The calibration curves for these metals and corresponding correlation coefficients ($R^2 > 0.99$) are presented in Fig. S2–S4 (ESI†), and the concentration of each metal element detected in the samples tested is given in Table S3 (ESI†). The BNB suspensions studied contained extremely low levels of metal traces similar to those detected in pure water, which implies that the observed nano-entities could not be attributed to the presence of metal contamination.

3.2.5 Drying of BNB suspensions. Drying experiments were performed to check for any non-volatile contaminants present in pure water or in BNB suspensions. Thus, 20 mL samples of pure water or BNB suspension were kept in glass flasks to completely evaporate in an oven at a temperature of 60 °C for 24 h. Any non-volatile substance contained in the original samples should have deposited during the drying process on the internal surfaces of the flasks. The empty flasks were then withdrawn and allowed to cool at room temperature before adding 20 mL of pure water. Each flask was left to soak for 24 h and then agitated to suspend any possible residue and the water was subsequently analysed by the NTA technique. Results shown in Fig. 7 confirm that, in all cases, no nano-entities were detected implying that the original samples contained no non-volatile impurities.

In conclusion, the various physical and chemical analytical techniques used above have produced multiple evidence which, taken together, provides conclusive proof that the nano-entities spontaneously formed by water–solvent mixing cannot be attributed to solvent nanodroplets or any type of common impurities or contamination as speculated in some literature reports[8–15] and, therefore, must be indeed gas-filled BNBs.

3.3 Fundamental questions relating to the existence and behaviour of BNBs in aqueous solvent solutions

On the basis of the findings of this study, the formation of BNBs in water–solvent mixtures raises a number of key questions which we will address, as follows.

3.3.1 Why is it not possible to form BNBs in a pure organic solvent? The corollary of the results discussed above (Fig. 3) is that BNBs cannot form in pure solvents. These results seem to suggest, therefore, that a pure organic solvent acts as a gas sink

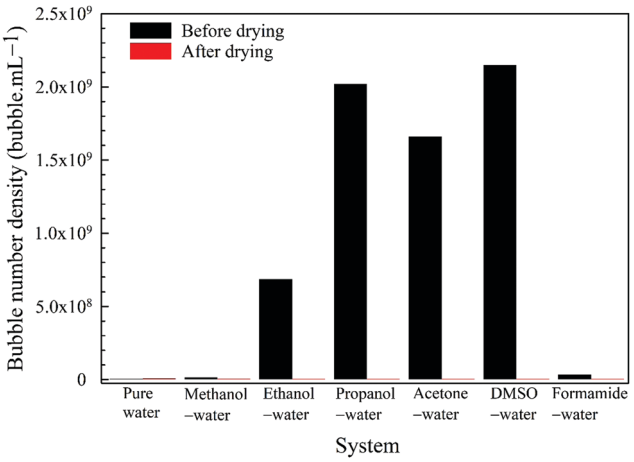

Fig. 7 Bubble number density before and after complete drying.

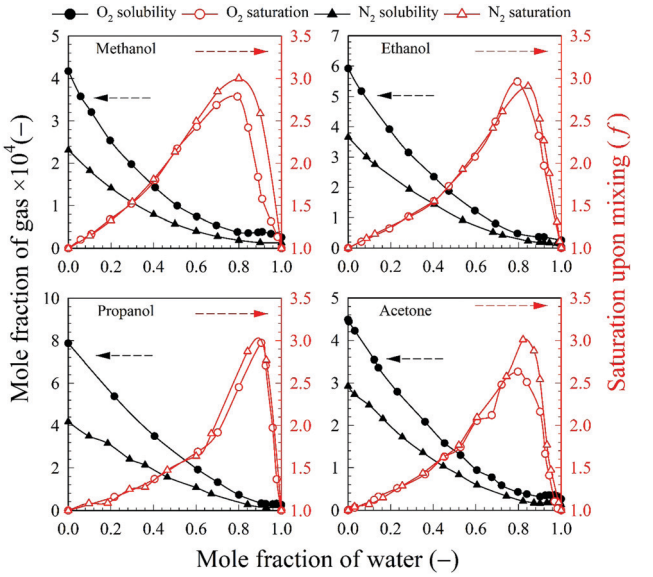

Fig. 8 Oxygen and nitrogen gas solubility and calculated saturation level resulting from organic solvent–water mixing at 293.15 K and 1 atm.

removing any excess gas from the solution and, consequently, it does not form nanobubbles. Hence, since BNBs exist in pure water, as reported by a number of scientific reports including our own,[5,6,17,48–50] then they should disappear at some organic solvent–water ratio, which is confirmed by the present results.

3.3.2 Why does the number density of BNBs reach a maximum at certain mole fraction of solvent? The mixing of pure saturated miscible solvents in water results in oversaturation of gas in the mixture. Data are available in the literature for the solubility of O_2 and N_2 in aqueous mixtures of the volatile solvents used here, *i.e.* methanol, ethanol, propanol and acetone.[51–53] It is, therefore, possible to calculate the level of saturation (f) that can be achieved by mixing these pure solvents with water at different mole fractions, which is defined as:[54]

$$f = \frac{X_m}{X_e} \quad (1)$$

and

$$X_m = \frac{X_w \times n_w + X_s \times n_s}{n_w + n_s} \quad (2)$$

where, X_m, X_e, X_w, X_s, n_w and n_s are, respectively, gas mole fraction obtained when the saturated solvent and water of a given mole fraction are mixed, gas mole fraction in that mixture,[51–53] mole fraction of gas in pure water, mole fraction of gas in pure solvent, mole fraction of water in solvent–water solution and mole fraction of solvent in solvent–water solution. The values of X_e for methanol, ethanol, propanol and acetone used in the calculations were obtained from Battino *et al.*[51,52] and Tsuji *et al.*[53] Note, however, that calculations for DMSO and formamide could not be conducted because similar solubility data could not be found.

The relevant O_2 and N_2 solubility data for methanol, ethanol, propanol and acetone are plotted in Fig. 8 together with the calculated f values. The O_2 solubility in methanol, ethanol propanol and acetone is, respectively, 16, 22, 30, and 17 times higher than in pure water; whereas the N_2 solubility is, respectively, 17, 27, 31, and 21 times higher than in pure water. However, as shown in Fig. 8, even though O_2 and N_2 are more soluble in pure solvent than in pure water, the maximum gas (O_2 and N_2) saturation level that can be achieved upon mixing corresponds to a high water mole fraction approximately in the range 0.80–0.90 depending on the type of solvent. Thus, the amount of gas contributed from the organic solvent phase is small and, at high solvent fractions, O_2 and N_2 have a much higher solubility in the aqueous mixture than in pure water. It is noteworthy that for each one of the volatile solvents considered, the water mole fraction yielding the highest level of gas saturation corresponds, within experimental error, to the solvent mole fraction at which the maximum bubble number density is observed (Fig. 3). This result seems to explain why the bubble number density is maximum at a certain mole fraction of solvent and falls off thereafter to zero as the solution becomes richer in solvent.

3.3.3 Why does the number density of BNBs vary with the type of solvent? Gas oversaturation is a useful parameter in determining the population of bubbles formed in the solution.[55] As discussed above, the solubility of atmospheric gases (O_2, N_2) in water has been observed to be lower than in aqueous solutions of methanol, ethanol, propanol and acetone and, therefore, gas oversaturation is expected to be higher in the presence of such solvents, thus resulting in the formation of BNBs. However, the same gases will have a different solubility depending on the organic solvent present (Fig. 8), which explains the differences in bubble number density achieved in different aqueous solvent solutions.

To illustrate these differences, the values of the maximum number density of BNBs formed in the aqueous solutions of these volatile solvents are compared in Fig. 9. Graphs of O_2 and N_2 solubility in the pure solvents are also plotted alongside these data. The bubble number density is highest for aqueous propanol followed successively order by aqueous ethanol, acetone and methanol. These results are consistent with the trends of variation of O_2 and N_2 solubility, *i.e.* propanol having relatively the highest gas solubility and methanol the lowest at any mole fraction.[56–58] A higher gas solubility in an organic solvent relative

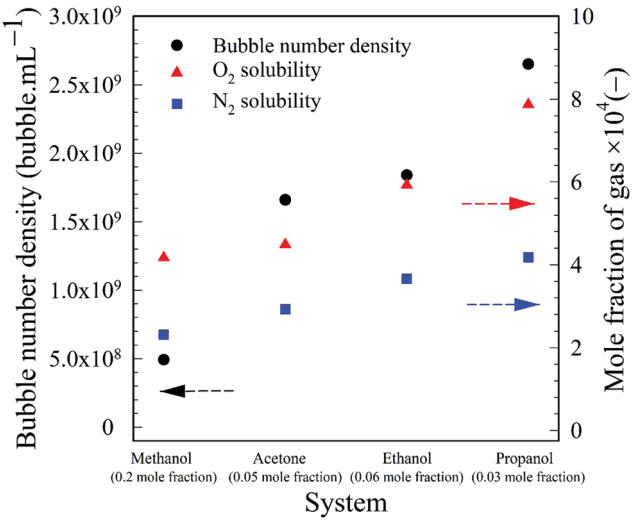

Fig. 9 Maximum bubble number density in aqueous volatile organic solvent solutions, plus O_2 and N_2 solubility values in the same pure solvents.

to water implies a higher gas availability for the nucleation of BNBs *via* gas oversaturation and, thus, a higher bubble number density at a lower mole fraction, *i.e.* 0.03 for propanol, 0.06 for ethanol, 0.05 for acetone and 0.2 for methanol (Fig. 3).

The low number of BNBs in methanol can be explained by its low gas solubility relative to water, and this argument can also be used to explain the extremely low number of BNBs in the case of formamide (Fig. 3). Formamide has the same oxygen solubility as pure water (~1.3 mM;[56] data for N_2 are not available) which means that the gas oversaturation is extremely low and, hence, the lack of gas release to form BNBs in the mixture.

In the case of DMSO the O_2 solubility is 0.33 mM, an order of magnitude lower than in water.[56] Nonetheless, there is considerable gas oversaturation in the mixture (albeit less than in the case of methanol, ethanol, propanol and acetone) which acts as the driving force behind the generation of BNBs. The solubility relative to water, therefore, is clearly one of the determining factors behind the nucleation of BNBs, but on its own does not fully explain why DMSO produces the highest BNB concentration amongst all the solvents considered here (Fig. 3). Consequently, the chemical structure of DMSO must also play an important direct or indirect role in stabilising the BNBs formed and, hence, influencing their number density. In the case of methanol, ethanol, propanol and acetone, the molecules of these solvents adsorb on the nanobubble interfaces and provide stability to the BNBs.[5,18] In the case of DMSO, it seems that the chemical structure of this solvent plays an even more important role in stabilising BNBs which seems to more than compensate for its comparatively low relative gas solubility. The exact mechanism by which this stabilising effect takes place in the case of DMSO is not *a priori* clear, however, and necessitates further study which is beyond the scope of this paper.

3.3.4 What is the stabilising mechanism of BNBs in aqueous organic solvent solutions? The zeta potential is a widely used measure of the magnitude of the surface charge of small

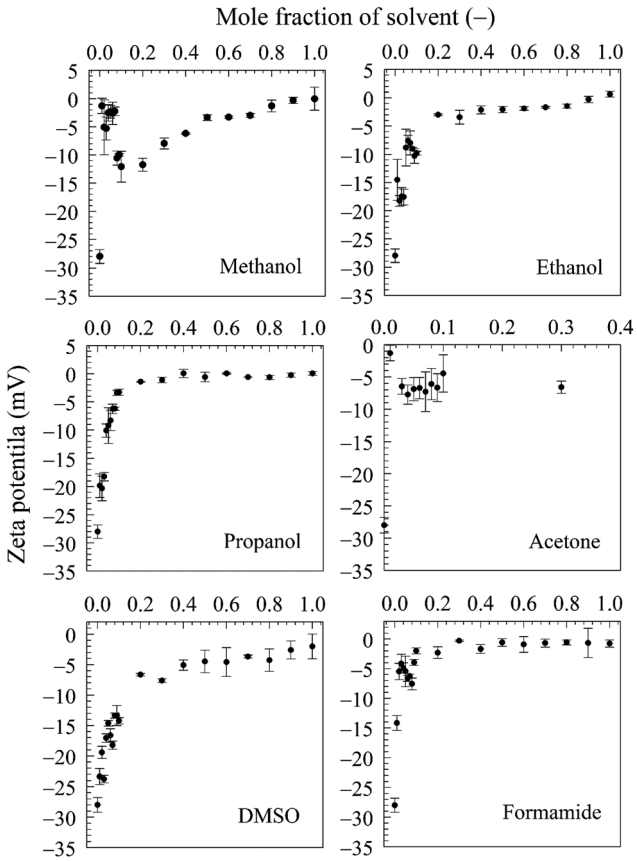

Fig. 10 Zeta potential of BNB suspensions.

dispersed entities, and the values measured for the BNB suspensions formed in the solvent–water mixtures are presented in Fig. 10. The zeta potential decreases sharply in magnitude with increasing mole fraction of solvent from a maximum value of −28 mV as previously reported for BNBs in pure water[17] to about −0.31 mV for methanol, −0.27 mV for ethanol, −0.27 mV for propanol, −2.61 mV for DMSO and −0.67 mV for formamide at the maximum mole fraction of 0.9 used, and −6.60 mV at the maximum mole fraction of 0.3 of acetone used.

The stability of BNBs in pure water is attributed to the presence of a significant charge afforded by the adsorption of hydroxyl ions on the interface. Although hydroxyl ions are present in water because of self-ionization, this is not the case in pure organic solvents which do not autoionize and, therefore, BNBs cannot exist in concentrated aqueous organic solvent solutions. Because of preferential adsorption of organic solvent molecules at the nanobubble interfaces, the surface charge of the nanobubbles decreases with solvent content, but the strong hydrogen bonding near their interfaces ensures their stability.[18] The observed reduction in zeta potential can, therefore, be explained by the increased adsorption of solvent molecules on the nanobubble interfaces.

Further evidence comes from the solvent evaporation experiment discussed above. After complete separation of the volatile solvents (methanol, ethanol, propanol, acetone) in the rotary evaporator, the zeta potential of BNBs in the remaining solvent-free water rose

to about −26.5 mV which is approximately the same as for nanobubbles produced in pure water (−28.0 mV). This result confirms that the molecules of these solvents do adsorb on the nanobubble interfaces and provide long-term stability to the BNBs.[5,18] For the solvents which produced stable nanobubbles, we monitored the BNB suspensions with the maximum bubble number density in 20 mL air-tight glass vials at room temperature. After a period of three months, the bubble number density and the bubble size distribution were unchanged within experimental error (± 1 to 5% depending on the solvent and its concentration).

4. Conclusions

The spontaneous formation of BNB suspensions and their stability in various aqueous organic solvent solutions have been studied. Multiple evidence has been provided which shows that the nano-entities formed by water–solvent mixing cannot be attributed to solvent nanodroplets, impurities or contamination and must therefore be gas-filled. Such BNBs enjoy long-term stability on the scale of months. The bubble number density increases sharply with solvent content, reaching a maximum at an intermediate solvent concentration depending on the type of solvent. This behaviour is attributed to gas oversaturation of water which is expected to be maximum at such mole fractions of solvent. Beyond this maximum, the bubble number density falls off sharply with no nanobubbles forming when the solvent content exceeds a certain mole fraction depending on the type of solvent. A pure organic solvent acts as a gas sink removing any excess gas from the solution and thus does not form nanobubbles. In an aqueous solvent solution, the gas solubility of the solvent relative to water is a determining factor in the number of BNBs formed. A solvent such as formamide with a gas solubility similar to that of water, *i.e.* approximately zero relative gas solubility, produces a negligible amount of BNBs. The stabilising effect afforded directly or indirectly to BNBs by the molecular structure of the solvent is another crucial factor in their formation and persistence. For solvents with a similar molecular structure (methanol, ethanol, propanol, acetone), a higher relative gas solubility leads to a maximum bubble number density at lower mole fractions. A solvent such as DMSO, whilst having a comparatively low relative gas solubility, produces considerably more BNBs.

Conflicts of interest

There are no conflicts of interest to declare.

Acknowledgements

This work was supported by EPSRC Grant EP/L025108/1.

References

1 J. Zhu, H. An, M. Alheshibri, L. Liu, P. M. J. Terpstra, G. Liu and V. S. J. Craig, *Langmuir*, 2016, **32**, 11203–11211.
2 K. Ohgaki, N. Q. Khanh, Y. Joden, A. Tsuji and T. Nakagawa, *Chem. Eng. Sci.*, 2010, **65**, 1296–1300.
3 A. Agarwal, W. J. Ng and Y. Liu, *Chemosphere*, 2011, **84**, 1175–1180.
4 S. H. Oh and J.-M. Kim, *Langmuir*, 2017, **33**, 3818–3823.
5 A. J. Jadhav and M. Barigou, *Langmuir*, 2020, **36**, 1699–1708.
6 N. Nirmalkar, A. W. Pacek and M. Barigou, *Langmuir*, 2018, **34**, 10964–10973.
7 P. B. August 2012, Big troubles over tiny bubbles, https://www.chemistryworld.com/features/big-troubles-over-tiny-bubbles/5306.article, accessed December 13, 2019.
8 F. Jin, J. Ye, L. Hong, H. Lam and C. Wu, *J. Phys. Chem. B*, 2007, **111**, 2255–2261.
9 M. Sedlák and D. Rak, *J. Phys. Chem. B*, 2013, **117**, 2495–2504.
10 M. Alheshibri and V. S. J. Craig, *J. Phys. Chem. C*, 2018, **122**, 21998–22007.
11 M. Alheshibri and V. S. J. Craig, *J. Colloid Interface Sci.*, 2019, **542**, 136–143.
12 M. Alheshibri, M. Jehannin, V. A. Coleman and V. S. J. Craig, *J. Colloid Interface Sci.*, 2019, **554**, 388–395.
13 A. Häbich, W. Ducker, D. E. Dunstan and X. Zhang, *J. Phys. Chem. B*, 2010, **114**, 6962–6967.
14 V. Leroy and T. Norisuye, *ChemPhysChem*, 2016, **17**, 2787–2790.
15 D. Rak, M. Ovadová and M. Sedlák, *J. Phys. Chem. Lett.*, 2019, **10**, 4215–4221.
16 P. E. Theodorakis and Z. Che, *Adv. Colloid Interface Sci.*, 2019, **272**, 101995.
17 N. Nirmalkar, A. W. Pacek and M. Barigou, *Soft Matter*, 2018, **14**, 9643–9656.
18 N. Nirmalkar, A. W. Pacek and M. Barigou, *Langmuir*, 2019, **35**, 2188–2195.
19 J. N. Meegoda, S. Aluthgun Hewage and J. H. Batagoda, *Environ. Eng. Sci.*, 2018, **35**, 1216–1227.
20 K. A. Mørch, *Interface Focus*, 2015, **5**, 20150006.
21 K. Ebina, K. Shi, M. Hirao, J. Hashimoto, Y. Kawato, S. Kaneshiro, T. Morimoto, K. Koizumi and H. Yoshikawa, *PLoS One*, 2013, **8**, e65339.
22 T. Temesgen, T. T. Bui, M. Han, T. Kim and H. Park, *Adv. Colloid Interface Sci.*, 2017, **246**, 40–51.
23 L. Hu and Z. Xia, *J. Hazard. Mater.*, 2018, **342**, 446–453.
24 A. Ushida, T. Hasegawa, T. Nakajima, H. Uchiyama and T. Narumi, *Exp. Therm. Fluid Sci.*, 2012, **39**, 54–59.
25 Z. Wu, X. Zhang, X. Zhang, G. Li, J. Sun, Y. Zhang, M. Li and J. Hu, *Surf. Interface Anal.*, 2006, **38**, 990–995.
26 Z. Wu, X. Zhang, X. Zhang, J. Sun, Y. Dong and J. Hu, *Chin. Sci. Bull.*, 2007, **52**, 1913–1919.
27 W. B. Cai, H. L. Yang, J. Zhang, J. K. Yin, Y. L. Yang, L. J. Yuan, L. Zhang and Y. Y. Duan, *Sci. Rep.*, 2015, **5**, 13725.
28 J. Du, X.-Y. Li, H. Hu, L. Xu, S.-P. Yang and F.-H. Li, *Sci. Rep.*, 2018, **8**, 3887.
29 J.-P. Wang, X.-L. Zhou, J.-P. Yan, R.-Q. Zheng and W. Wang, *Oncotarget*, 2017, **8**, 78153–78162.
30 N. Matsuki, T. Ishikawa, S. Ichiba, N. Shiba, Y. Ujike and T. Yamaguchi, *Int. J. Nanomed.*, 2014, **9**, 4495–4505.

31 S. Liu, S. Oshita, Y. Makino, Q. Wang, Y. Kawagoe and T. Uchida, *ACS Sustainable Chem. Eng.*, 2016, **4**, 1347–1353.
32 S. Liu, Y. Kawagoe, Y. Makino and S. Oshita, *Chem. Eng. Sci.*, 2013, **93**, 250–256.
33 S. H. Oh, J. G. Han and J.-M. Kim, *Fuel*, 2015, **158**, 399–404.
34 S. H. Oh, S. H. Yoon, H. Song, J. G. Han and J.-M. Kim, *Int. J. Hydrogen Energy*, 2013, **38**, 14849–14853.
35 F. Y. Ushikubo, T. Furukawa, R. Nakagawa, M. Enari, Y. Makino, Y. Kawagoe, T. Shiina and S. Oshita, *Colloids Surf., A*, 2010, **361**, 31–37.
36 R. Etchepare, H. Oliveira, M. Nicknig, A. Azevedo and J. Rubio, *Miner. Eng.*, 2017, **112**, 19–26.
37 S.-H. Cho, J.-Y. Kim, J.-H. Chun and J.-D. Kim, *Colloids Surf., A*, 2005, **269**, 28–34.
38 J.-Y. Kim, M.-G. Song and J.-D. Kim, *J. Colloid Interface Sci.*, 2000, **223**, 285–291.
39 W. B. Zimmerman, V. Tesař and H. C. H. Bandulasena, *Curr. Opin. Colloid Interface Sci.*, 2011, **16**, 350–356.
40 A. K. A. Ahmed, C. Sun, L. Hua, Z. Zhang, Y. Zhang, W. Zhang and T. Marhaba, *Chemosphere*, 2018, **203**, 327–335.
41 S.-T. Lou, Z.-Q. Ouyang, Y. Zhang, X.-J. Li, J. Hu, M.-Q. Li and F.-J. Yang, *J. Vac. Sci. Technol., B: Microelectron. Nanometer Struct. – Process., Meas., Phenom.*, 2000, **18**, 2573–2575.
42 S. Yang and A. Duisterwinkel, *Langmuir*, 2011, **27**, 11430–11435.
43 S. Peng, T. L. Mega and X. Zhang, *Langmuir*, 2016, **32**, 11265–11272.
44 S. R. German, X. Wu, H. An, V. S. J. Craig, T. L. Mega and X. Zhang, *ACS Nano*, 2014, **8**, 6193–6201.
45 W. Drost-Hansen, *Science*, 1969, **166**, 861.
46 B. Louise Mojet, S. Dalgaard Ebbesen and L. Lefferts, *Chem. Soc. Rev.*, 2010, **39**, 4643–4655.
47 M. Mekala and V. R. Goli, *Data in Brief*, 2018, **18**, 947–960.
48 K. Yasuda, H. Matsushima and Y. Asakura, *Chem. Eng. Sci.*, 2019, **195**, 455–461.
49 Q. Wang, H. Zhao, N. Qi, Y. Qin, X. Zhang and Y. Li, *Sci. Rep.*, 2019, **9**, 1–9.
50 J. Jin, Z. Feng, F. Yang and N. Gu, *Langmuir*, 2019, **35**, 4238–4245.
51 R. Battino, T. R. Rettich and T. Tominaga, *J. Phys. Chem. Ref. Data*, 1984, **13**, 563–600.
52 R. Battino, T. R. Rettich and T. Tominaga, *J. Phys. Chem. Ref. Data*, 2009, **12**, 163.
53 K. Tsuji, K. Ichikawa, H. Yamamoto and J. Tokunaga, *Kagaku Kogaku Ronbunshu*, 1987, **13**, 825–830.
54 P. S. Epstein and M. S. Plesset, *J. Chem. Phys.*, 1950, **18**, 1505–1509.
55 H. Liu and G. Cao, *Sci. Rep.*, 2016, **6**, 23936.
56 C. Franco and J. Olmsted, *Talanta*, 1990, **37**, 905–909.
57 D. Dvoranová, Z. Barbieriková and V. Brezová, *Molecules*, 2014, **19**, 17279–17304.
58 M. Quaranta, M. Murkovic and I. Klimant, *Analyst*, 2013, **138**, 6243–6245.